DOI: 10.1002/((No. admi.201801291))
Article type: Full paper

Atomic Layer Deposition of Intermetallic Co_3Sn_2 and Ni_3Sn_2 Thin Films

Katja Väyrynen, Timo Hatanpää, Miika Mattinen, Kenichiro Mizohata, Kristoffer Meinander, Jyrki Räisänen, Joosep Link, Raivo Stern, Mikko Ritala and Markku Leskelä*

K. Väyrynen, T. Hatanpää, M. Mattinen, Prof. M. Ritala, Prof. M. Leskelä
Department of Chemistry, University of Helsinki, P.O. Box 55, FI-00014 Helsinki, Finland
E-mail: mikko.ritala@helsinki.fi
Dr. K. Mizohata, Dr. K. Meinander, Prof. J. Räisänen
Department of Physics, University of Helsinki, P.O. Box 64, FI-00014 Helsinki, Finland
J. Link, Prof. R. Stern
National Institute of Chemical Physics and Biophysics, Akadeemia tee 23, 12618 Tallinn, Estonia

Keywords: Co_3Sn_2, Ni_3Sn_2, intermetallics, thin films, atomic layer deposition

Intermetallics form a versatile group of materials that possess unique properties ranging from superconductivity to giant magnetoresistance. The intermetallic Co–Sn and Ni–Sn compounds are promising materials for magnetic applications as well as for anodes in lithium- and sodium-ion batteries. Herein, we present a method for the preparation of Co_3Sn_2 and Ni_3Sn_2 thin films using diamine adducts of cobalt(II) and nickel(II) chlorides, $CoCl_2$(TMEDA) and $NiCl_2$(TMPDA) (TMEDA = N,N,N’,N’-tetramethylethylenediamine, TMPDA = N,N,N’,N’,-tetramethyl-1,3-propanediamine) combined with tributyltin hydride (TBTH). The films were grown by atomic layer deposition (ALD), a technique that enables conformal film deposition with sub-nm thickness control. The Co_3Sn_2 process fulfilled the typical ALD qualifications, such as self-limiting growth, excellent film uniformity, and conformal coverage of a trench structure. XRD measurements showed reflections characteristic to the hexagonal Co_3Sn_2 phase, which confirmed that the films were, indeed, intermetallic instead of being mere alloys of Co and Sn. ToF-ERDA measurements confirmed the intermetallic composition and showed that the films were extremely pure with impurity levels each below 1.0 at.%. Ni_3Sn_2 films similarly exhibited the expected XRD reflections for the intermetallic phase and were of high

purity in composition measurements. The Co_3Sn_2 films showed magnetic hysteresis with high coercivity values exceeding 500 Oe, indicating great potential in terms of applicability of the films.

1. Introduction

Intermetallics are compounds that comprise two or more metal elements with a defined stoichiometry and an ordered crystal structure.[1,2] Intermetallic compounds display a specific crystal structure, which is distinct from metal alloys that exhibit the crystal structures of the participating metal components. An intermetallic compound is formed when the bonds between the dissimilar atoms are stronger than the bonds between the atoms of the same element.

Because of their specific structure, intermetallic compounds usually exhibit unique physical and chemical properties that are potentially superior to their disordered alloy analogues and the pure metals. Such properties include, for example, magnetoresistance,[3,4] superconductivity,[5–7] enhanced catalytic activity,[8,9] and hydrogen storage capability.[10] Intermetallics and alloys containing Co or Ni and Sn with varying stoichiometry have mostly been studied as anode materials for Li- and Na-ion batteries.[11–19] As ferromagnetic materials, they also show potential for magnetic devices.[20–22] Furthermore, intermetallic Co–Sn and Ni–Sn compounds have also been studied for catalytic purposes.[23–26]

For future applications like nanoelectronic devices, it is pivotal to be able to control the thickness and composition of thin films with sub-nm accuracy. Atomic layer deposition (ALD) is a thin film preparation method based on repeated, saturative and irreversible surface reactions between alternately supplied gaseous precursors ensuring self-limiting growth of the desired material.[27,28] Owing to the self-limiting growth mechanism, ALD can be used to deposit uniform thin films over complex structures in a controlled and reproducible manner.

No previous reports on the ALD of intermetallic Co_3Sn_2 or Ni_3Sn_2 thin films are found in the literature, and the ALD of other intermetallic compounds has also been scarce if existent at all. Intermetallic phases in Pt–In,[29] Pt–Sn,[30] and Ni–Fe[31] systems have been obtained by the postdeposition reduction of the corresponding ALD oxides. There are also some ALD studies on metal alloys, such as Pt–Ir,[32] Pd–Pt,[33–35] Ru–Pt,[36] Ru–Co,[37] Co–W,[38,39] Co–Pt,[40] Ru–Mn,[41] and Cu–Mn,[42] but no reports exist on materials exhibiting a specific intermetallic structure. Co–Sn and Ni–Sn with varying stoichiometry, including the intermetallic Co_3Sn_2 and Ni_3Sn_2 phases, have generally been prepared by, for example, ball milling,[43] melting,[24] different solution-based techniques,[26,44,45] solvo- and hydrothermal routes,[12,14–16,18,20] electrodeposition,[17,19,21,46] sputtering,[47] and electron beam evaporation.[11] Chemical vapor deposition (CVD) has been employed to deposit an alloy of Co and Sn with 1:1 stoichiometry using two single-source precursors: $Me_3SnCo(CO)_4$ and $Ph_3SnCo(CO)_4$. The films contained only a minor constituent of Co_3Sn_2.[48] Ni_3Sn, Ni_3Sn_2, and Ni_3Sn_4 have also been deposited by CVD using $SnMe_4$ and Ni substrates followed by hydrogen treatment at high temperatures.[23,25]

Herein, we introduce the direct ALD of intermetallic Co_3Sn_2 and Ni_3Sn_2 thin films using a combination of diamine adducts of the corresponding metal(II) chlorides and tributyltin hydride (TBTH) as precursors (**Figure 1**). A full ALD study on the growth properties of Co_3Sn_2 at low temperatures of 170–200 °C will be described. Results obtained by thorough characterization of the films indicate great potential in terms of device integration. Finally, we believe that the approach shown here can be applied to other intermetallics as well, which opens up interesting perspectives for new applications of ALD.

2. Results

2.1. Precursor Selection

In our previous article we showed that as a polymeric, poorly volatile compound, $CoCl_2$ is an unsuitable precursor for ALD.[49] By simply adding a bidentate Lewis base molecule, TMEDA, to $CoCl_2$, a monomeric adduct compound, $CoCl_2$(TMEDA), with suitable precursor properties was realized. This adduct combined with water was used successfully to deposit CoO. $CoCl_2$(TMEDA) was shown to sublime intact at temperatures of 150–200 °C under reduced pressure. The ALD experiments were conducted at temperatures up to 300 °C without signs of major thermal decomposition, though TGA (thermogravimetric analyses) suggested that as a bulk material, some dissociation of the adduct-forming TMEDA ligand took place already around 200 °C. When studying the amine adducts of $NiCl_2$, it became evident that TMEDA was not a suitable adduct-forming ligand for nickel, while TMPDA was. From the literature it is known that TMEDA reacts with $NiCl_2$ to form $NiCl_2(TMEDA)_2$ as well as cluster and ion pair compounds $[Ni_3Cl_5(TMEDA)_3]Cl$ and $[Ni_3Cl_5(TMEDA)_3]_2[NiCl_4]$.[50] $NiCl_2$(TMEDA) has not been isolated. Considering the thermal properties, we observed that $NiCl_2(TMEDA)_2$ releases TMEDA upon heating and forms $[Ni_3Cl_5(TMEDA)_3]Cl$ that sublimes with a very low yield. The clusters or ion pair compounds most likely decompose when heated, and part of the compound sublimes as $NiCl_2$(TMEDA). The properties of the sublimate are identical with those of $[Ni_3Cl_5(TMEDA)_3]Cl$. In contrast, $NiCl_2$(TMPDA) is a monomeric compound[51] that shows almost quantitative sublimation at 150–175 °C/0.4 mbar. The synthesis and characterization of $NiCl_2$(TMPDA) and $NiCl_2(TMEDA)_2$ are given in the Supporting Information.

Tributyltin hydride (TBTH) is a highly air and moisture sensitive liquid. TGA conducted on TBTH suggests that the compound evaporates and is thermally stable up to at least 200 °C. TBTH has not been studied in ALD before.

2.2. Film Deposition

The growth characteristics of the Co_3Sn_2 process are depicted in **Figure 1**. Self-limiting growth with a high rate of 0.9 Å/cycle was observed with respect to both $CoCl_2$(TMEDA) and TBTH pulse lengths at 180 °C (Figure 1b and 1c). The purge time had no significant effect on the growth rate (Figure S5 in the Supporting Information). Film thickness was linearly dependent on the number of cycles, another indication of ideal ALD behavior (Figure 1d), though some nucleation delay could be observed within the very first cycles. As is often observed in the ALD of metals, the growth rate was strongly dependent on the deposition temperature, and the rate increased almost linearly from 0.7 to 1.3 Å/cycle within the range of 170–200 °C (Figure 1e). The process was studied at low temperatures (≤200 °C) to minimize agglomeration of the film, a common problem in metal ALD, and to avoid decomposition of TBTH. $CoCl_2$(TMEDA) has been shown to be thermally stable up to ~300 °C.[49] The lower limit of 170 °C was dictated by the source temperature of $CoCl_2$(TMEDA), also 170 °C.

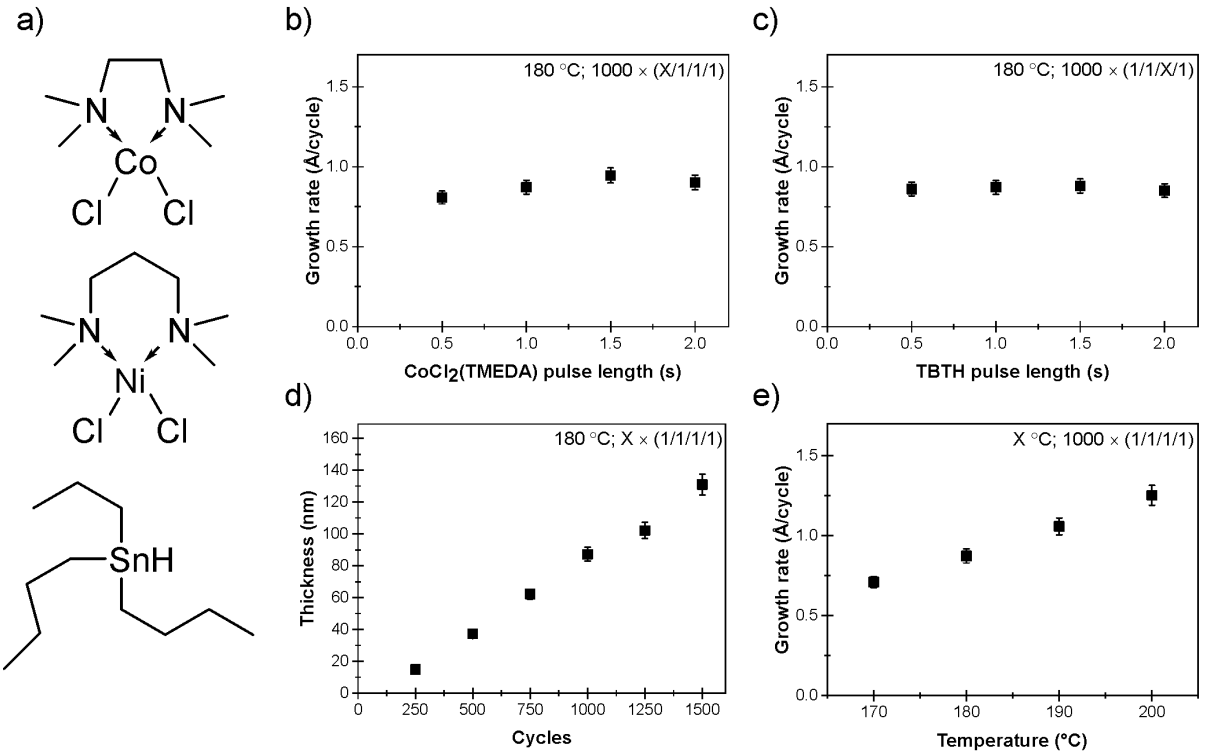

Figure 1. a) Schematic structures of the precursors used in this study and growth characteristics of the Co_3Sn_2 process: growth rate as a function of b) $CoCl_2$(TMEDA) pulse

length, c) TBTH pulse length, d) film thickness as a function of cycle count, and e) growth rate with respect to deposition temperature. The labels depict the deposition conditions (temperature, cycle count, and pulsing sequence in seconds).

2.3. Film Characterization

The Co_3Sn_2 films were studied for their uniformity, conformality, and morphology (**Figure 2**). Thickness uniformity of an 87 nm film deposited at 180 °C was evaluated across the 5 cm × 5 cm substrate (Si with native oxide). As Figure 2a shows, the film thickness was almost the same both at the inlet edge of the substrate, that is, the point where the precursors first meet the substrate, and close to the exhaust. Only slight variation within the 5% error limits was seen indicating excellent film uniformity. Like with any proper ALD process, conformal coverage of a structured Si substrate was achieved using the $CoCl_2$(TMEDA) + TBTH precursor combination. Figure 2b illustrates a ~40 nm Co_3Sn_2 film deposited on trench structures with different dimensions. The SEM image shows good step coverage and uniform trench fill.

Top-view SEM images of Co_3Sn_2 films deposited on native oxide-terminated Si with varying cycle counts at 180 °C are shown in Figure 2c. Characteristic to the ALD of metals, also the Co_3Sn_2 films exhibited quite strong agglomeration during nucleation. Even so, a film of only 15 nm thickness deposited with 250 cycles formed a continuous network of Co_3Sn_2 over the substrate. Full coverage of the substrate was observed with a film thickness of 37 nm (500 cycles). Initially, the grain size increased with increasing cycle count and thickness. No significant change in the grain size was observed anymore between the 87 and 131 nm films. The roughness of the Co_3Sn_2 films was assessed by AFM. Figure S6 (Supporting Information) shows AFM images of 15, 37, and 87 nm Co_3Sn_2 films deposited at 180 °C. All the films were rough, with the R_q values being 4.8, 5.5, and 7.1 nm in the order of increasing film thickness. The 15 and 37 nm films had similar roughnesses likely due to the discontinuity of the former as seen in Figure 2c. The 37 nm sample also exhibited some higher grains. The

extent of these higher grains increased with increasing film thickness making the 87 nm film clearly the roughest.

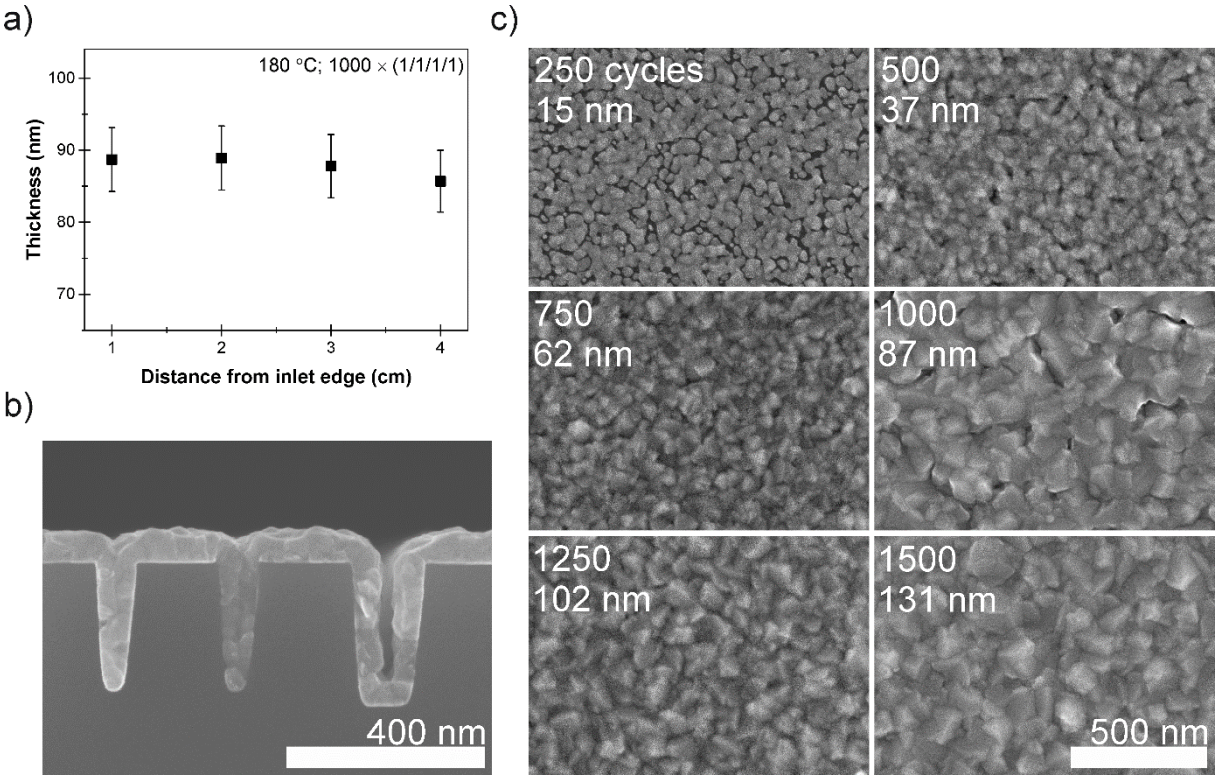

Figure 2. a) Thickness uniformity of an 87 nm Co_3Sn_2 film. b) Co_3Sn_2 of ~40 nm thickness deposited on a structured Si trench substrate. c) SEM images of Co_3Sn_2 films deposited with different cycle counts at 180 °C.

The Co_3Sn_2 films were also analyzed in terms of crystal structure and chemical composition (**Figure 3**). Figure 3a depicts an X-ray diffractogram of an 87 nm Co_3Sn_2 film deposited at 180 °C. The film was highly crystalline with reflections corresponding to the specific structure of the intermetallic, hexagonal Co_3Sn_2. Some reflections could be attributed not only to Co_3Sn_2 but also to the cubic Co (44.2°) or tetragonal β-Sn metal phases (30.6°, 43.9°). However, the rest of the reflections characteristic to Co and Sn are missing pointing toward the intermetallic crystal structure.

Film composition was examined by ToF-ERDA. The elemental depth profiles of a 131 nm Co_3Sn_2 thin film are presented in Figure 3b. The film was of high purity with negligible

amounts of H, C, and O (each below 1.0 at.%). Notably, no chlorine was detected in the film, despite it being a constituent of the Co precursor. The high purity suggests fast and complete reactions between the precursors. Upon the adsorption of $CoCl_2$(TMEDA), the adduct is most likely lost leaving the surface with chlorinated cobalt atoms. The butyl groups of TBTH may then act as chlorine scavengers releasing volatile 1-chlorobutane and hydrogen (Equation 1). In situ studies to verify the reaction mechanism are underway.

$$3\ CoCl_2 + 2\ Bu_3SnH \rightarrow Co_3Sn_2 + 6\ BuCl + H_2 \quad (1)$$

According to Figure 3b, the Sn content seems to increase and the Co content to decrease toward the surface of the film. This is in correlation with the Co:Sn ratio being, in general, close to 70:30 in thinner films and 60:40 in thicker films (Figure 3c). No clear trend was observed regarding the Co:Sn ratio with respect to the deposition temperature or precursor pulse lengths. There was slight variation between the samples most likely arising from the uncertainty of the EDS measurement.

The chemical states of both Co and Sn on the surface of an 87 nm Co_3Sn_2 film deposited at 180 °C were identified by XPS using the Co 2p and Sn 3d core levels, respectively (Figure 3d). Signals deriving from surface oxidation (CoO, $Co(OH)_2$, SnO, and SnO_2) were inevitable as the samples had been exposed to air and no sputtering was done prior to or during the measurement. The high amounts of metallic Co and Sn indicate, however, that in the film bulk, the oxidation state of both metals is close to zero. Signals corresponding to Co metal are seen at binding energies of 778 and 793 eV (Co $2p_{3/2}$ and Co $2p_{1/2}$, respectively). The peaks at binding energies of 781 and 797 eV as well as the shake-up satellites at 786 and 803 eV arise from the oxidized surface species.[52] The Sn metal peaks are visible at 485 and 493 eV in the Sn 3d spectrum ($3d_{5/2}$ and $3d_{3/2}$). The signals at 486 and 495 eV as well as the low intensity peaks at 488 and 497 eV derive from surface oxidation. The relative amount of Sn was high

with respect to Co; the Sn:Co ratios measured by XPS were above 2.6. Similarly, a high Sn:Ni ratio was also observed in the case of Ni_3Sn_2 (Figure S7 in the Supporting Information). The distorted atomic ratios can also be attributed to the surface oxidation; SnO_x is known to segregate on the surface and at grain boundaries, which causes the high intensity Sn signals.[53,54]

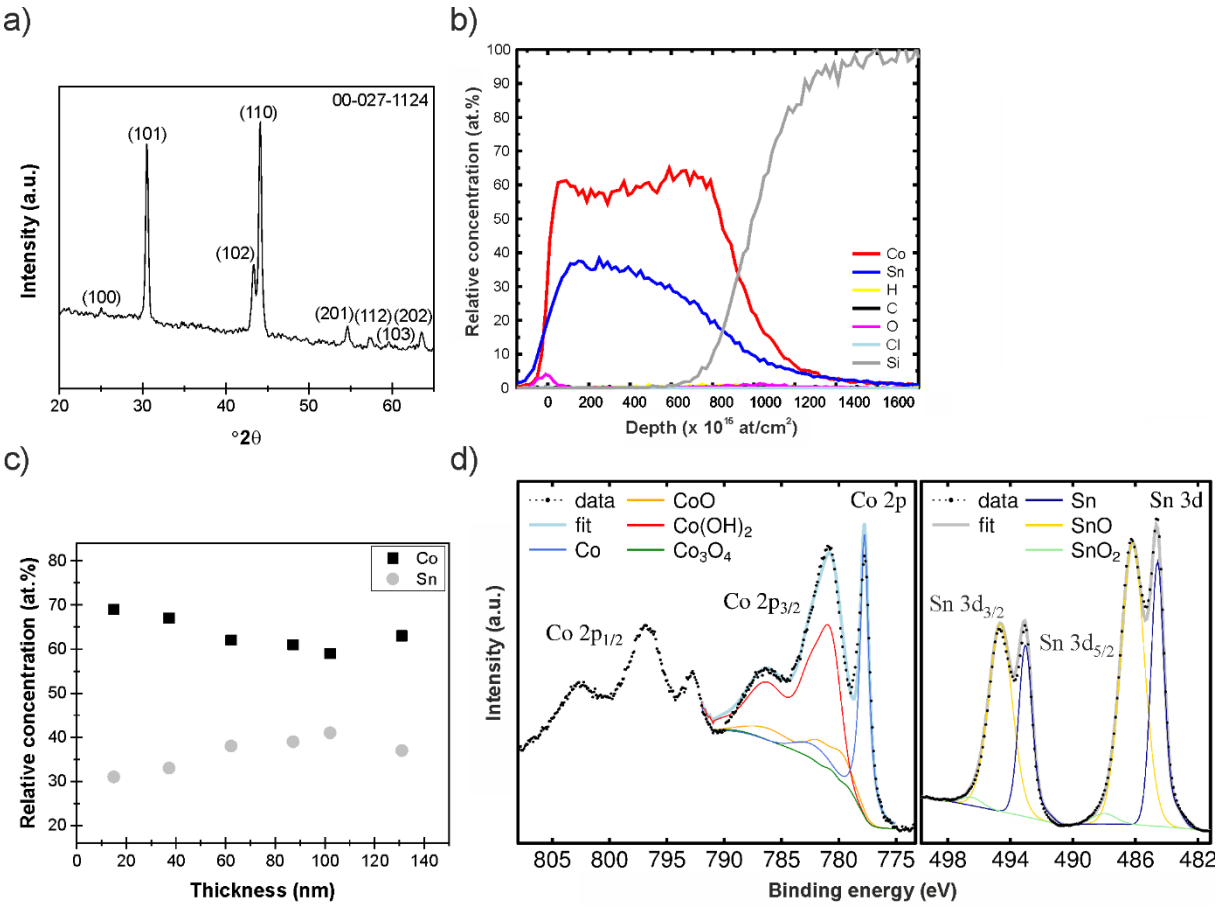

Figure 3. Characterization of Co_3Sn_2 films deposited at 180 °C. a) Grazing incidence X-ray diffractogram of an 87 nm Co_3Sn_2 film. The indices correspond to the hexagonal, intermetallic Co_3Sn_2 structure. b) ToF-ERDA depth profile of a 131 nm Co_3Sn_2 film. c) The atomic percentages (EDS) of Co and Sn in films of different thicknesses. d) XPS data from the surface of an 87 nm Co_3Sn_2 thin film.

Both magnetic and electrical measurements gave promising results for the Co_3Sn_2 films (**Figure 4**). Vibrating sample magnetometry was used to analyze the magnetic properties of the Co_3Sn_2 thin films of different thicknesses deposited on Si with native oxide at 180 °C. The measurements were executed in the plane of the film surface at room temperature. Figure 4a

shows the hysteresis loops of the samples. The reference Si exhibited linear diamagnetic behavior indicating that the substrate was free from magnetic impurities. All the films showed magnetic hysteresis. The 37 and 87 nm films had similar coercivity values of 485 and 510 Oe, respectively. The 15 nm film exhibited a lower coercivity of 320 Oe most likely resulting from the noncontinuous structure of the film. In comparison, the coercivity observed by Yi et al. for Co_3Sn_2 nanoparticles was only 131.5 Oe.[20] Pereira and co-workers also reported much lower coercivity values, but the films were far less crystalline than the films shown here and consisted of multiple Co–Sn phases.[21] The coercivity value reported for an ALD Co film was 230 Oe.[55] The Co film in that report was deposited using $Co(^{iPr}AMD)_2$ (^{iPr}AMD = N,N'-diisopropylacetamidinate) and H_2 as precursors.

The thickest film of 87 nm was also measured along different edges of the film as well as perpendicular to the film surface (Figure S8 in the Supporting Information). The two in-plane measurements overlapped almost completely showing that the film is isotropic in these directions. It was more difficult to magnetize the sample in the out-of-plane direction indicating a preferential anisotropy toward the film plane.

Resistivity of the Co_3Sn_2 films was measured as a function of film thickness (Figure 4b). At the lowest, a resistivity of 74 μΩcm was measured for a 15 nm film. The resistivity increased with increasing film thickness, and a value of 157 μΩcm was measured for a 102 nm film. Usually, resistivity is the highest for very thin films and decreases with increasing film thickness until a constant value is reached. The opposite trend observed in this case can be explained by the changing Co:Sn ratio seen in Figure 3c. The thinnest film that exhibited the lowest resistivity had the highest Co:Sn ratio (70:30). The 62 and 87 nm films exhibited similar resistivities due to their similar Co:Sn ratios. The Co:Sn ratio of the thickest film was the lowest (59:41) and, consequently, the resistivity was the highest. Resistivity has not generally been assessed in the context of Co_3Sn_2; thus, no literature value for bulk resistivity could be found. Sun et al. reported much lower resistivity values of 12–25 μΩcm for their

Co–Sn system, but the films exhibited 1:1 Co:Sn stoichiometry and only a minor constituent of Co_3Sn_2.[48] Resistivity has typically not been the measure of highest interest for Co_3Sn_2, as the material has mostly been studied for Li- and Na-ion batteries as well as magnetic applications.

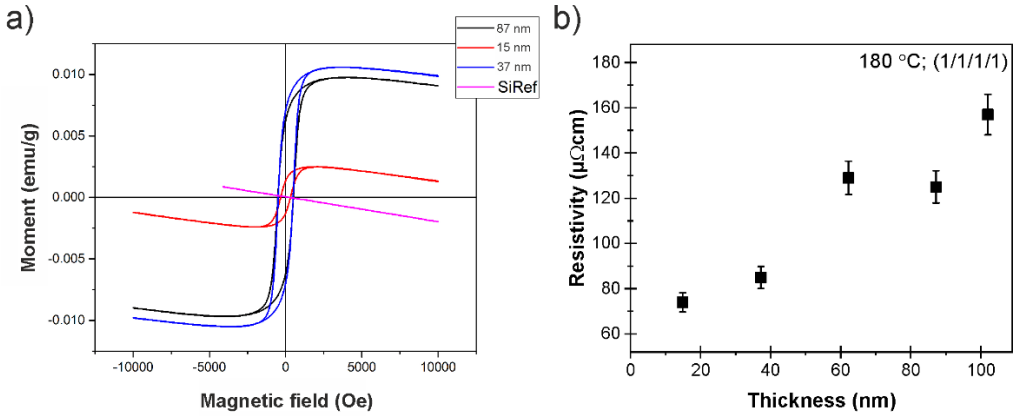

Figure 4. Magnetic and electrical properties of Co_3Sn_2 thin films. a) Magnetization of 15, 37, and 87 nm Co_3Sn_2 thin films and their Si support as a reference as a function of magnetic field at ambient temperature. b) Co_3Sn_2 resistivity as a function of film thickness.

Similarly to $CoCl_2$(TMEDA), a diamine adduct of nickel(II) chloride, $NiCl_2$(TMPDA), could be used to deposit Ni_3Sn_2 thin films upon combination with tributyltin hydride. A growth rate of 1.3 Å/cycle was measured at a low temperature of 160 °C. Further studies regarding the growth characteristics are underway. As with Co_3Sn_2, reflections corresponding to the intermetallic Ni_3Sn_2 phase were observed by XRD (Figure S9 in the Supporting Information). Figure S10 (Supporting Information) shows an SEM image of a 127 nm Ni_3Sn_2 film the appearance of which resembles that of Co_3Sn_2. According to ToF-ERDA, the 127 nm Ni_3Sn_2 film deposited at 160 °C exhibited high purity and low levels of H, C, O, and N (Table S1 in the Supporting Information). As with Co_3Sn_2, no chlorine was detected in the Ni_3Sn_2 film. Based on our preliminary studies, it seems that the ALD of Co_3Sn_2 and Ni_3Sn_2 films is not restricted to metal halide precursors only. Ni_3Sn_2 films could be deposited also with $Ni(dmap)_2$ (dmap = dimethylamino-2-propoxide) and TBTH at low temperatures of 140–

180 °C. Furthermore, by using different metal precursors, the same approach may be applied to the deposition of other types of intermetallic compounds as well. Winter's group recently published a report on the ALD of aluminum metal using $AlCl_3$ and an aluminum dihydride as precursors.[56] By combining the aluminum dihydride, or any other volatile aluminum hydride, with another metal precursor, an aluminum comprising intermetallic film could possibly be deposited. In addition to tin hydrides and alanes, other metal and semimetal hydrides, such as germanes, or some metal-containing reactants could be selected providing nearly limitless opportunities in terms of undiscovered ALD chemistries.

3. Conclusion

To summarize, we have described the ALD of intermetallic Co_3Sn_2 and Ni_3Sn_2 thin films. The films were deposited using diamine adducts of cobalt(II) and nickel(II) chlorides combined with tributyltin hydride at low temperatures below 200 °C. The Co_3Sn_2 process exhibited a self-limiting growth mechanism, and a saturated growth rate of 0.9 Å/cycle was observed with respect to both precursors. Excellent film uniformity and good step coverage were also demonstrated. XRD and ToF-ERDA showed that the films were, indeed, intermetallic Co_3Sn_2 and Ni_3Sn_2 — not just alloys of the metals in question. The films exhibited high purity and only small traces of H, C, and O (each below 1.0 at.%). Based on magnetic measurements, the Co_3Sn_2 films show great potential for the development of magnetic applications. We have also shown that it is possible to extend the deposition of intermetallic films from halides to other types of metal precursors. Lastly, by choosing different metals, new ALD processes can be developed for other intermetallic compounds as well breaking further ground in the exciting field of intermetallics ALD.

4. Experimental Section

Film Deposition: All the film depositions were executed in a hot-wall cross-flow F-120 ALD reactor (ASM Microchemistry). Nitrogen (AGA, 99.999 %; H_2O, ≤3 ppm; O_2, ≤3 ppm) was used as both the carrier and purge gas. The reactor pressure during the experiments was in the order of ~10 mbar. $CoCl_2$(TMEDA) was synthesized according to the procedure reported previously,[49] and the synthesis of $NiCl_2$(TMPDA) is described in the Supporting Information. Tributyltin hydride (TBTH) was purchased from Alfa Aesar. All the precursors were sublimed from open glass boats held inside the reactor at 170, 157, and 30 °C for the Co, Ni, and Sn precursors, respectively. The pulse and purge times, controlled by inert gas valving, were varied from 0.5 to 2.0 s. All the experiments, apart from the purge series itself, were carried out with 1.0 s purges. The Co_3Sn_2 process was studied on 5 cm × 5 cm Si(100) and soda lime glass substrates at 170–200 °C.

Film Characterization: Film thicknesses were measured on native oxide-terminated Si(100) substrates by energy-dispersive X-ray spectrometry (EDS) using an Oxford INCA 350 microanalysis system connected to a Hitachi S-4800 scanning electron microscope (SEM). The electron energy was 20 keV. The thicknesses were determined from Co Kα, Ni Kα, and Sn Lα X-ray lines with the GMRFILM program assuming a density of 9.08 g/cm^3 for Co_3Sn_2.[57] The density of a ~40 nm Co_3Sn_2 film was verified by X-ray reflectivity (XRR, PANalytical X'Pert Pro MPD X-ray diffractometer). The same density (9.08 g/cm^3) was used as an approximation also for Ni_3Sn_2. The uncertainty of each thickness measurement was estimated at 5%.

SEM was also employed to study film conformality and morphology. Atomic force microscopy (AFM) images for analyzing surface roughness were recorded using a Veeco Multimode V instrument. Tapping mode images were captured in air using Si probes with a nominal tip radius of 10 nm and a nominal spring constant of 3 N/m (RFESP from Bruker).

The images were flattened to remove artefacts caused by sample tilt and scanner bow. Roughness was calculated as a root-mean-square value (R_q) from 2 μm × 2 μm images.

Film crystallinity was evaluated by X-ray diffraction (XRD) using parallel beam optics and grazing incidence measurement geometry. The incident angle of the Cu Kα (λ = 1.54 Å) radiation was 1°.

Elemental composition was examined by time-of-flight elastic recoil detection analysis (ToF-ERDA) using a 40 MeV $^{79}Br^{7+}$ ion beam for Co_3Sn_2 and a 50 MeV beam for Ni_3Sn_2. A more detailed description of the setup is reported in the literature. Oxidation states of Co, Ni, and Sn were identified by X-ray photoelectron spectroscopy (XPS) using an Omicron ARGUS spectrometer operated at a 20 eV pass energy. The samples were irradiated by a Mg source (Kα line) emitting X-rays at an energy of 1253.6 eV. No sputtering was done prior or during the XPS. The C 1s peak of ambient hydrocarbons (284.8 eV) was used for energy calibration. Peaks were fitted with the CasaXPS software package.

To examine the magnetic properties of Co_3Sn_2, the vibrating sample magnetometer (VSM) option of a Quantum Design PPMS was used. All measurements were performed at room temperature. Magnetic field was changed in small steps and in non-overshoot mode. At each field, magnetic moment was averaged for 10 seconds (10 s × 40 Hz = 400 counts). The mass of the sample included both the film and the Si substrate.

A four-point probe (CPS Probe Station, Cascade Microtech combined with a Keithley 2400 SourceMeter) was used to measure the resistivity of Co_3Sn_2 films of different thicknesses deposited on soda lime glass substrates at 180 °C. First, the sheet resistance was measured and then multiplied by film thickness to obtain the resistivity. Film thickness on soda lime glass was the same as on Si with native oxide.

Supporting Information
Supporting Information is available from the Wiley Online Library or from the author.

Acknowledgements
Funding from ASM Microchemistry Oy and Finnish Centre of Excellence in Atomic Layer Deposition is gratefully acknowledged. J.L. and R.S. wish to thank the Estonian Research Agency grant PRG4 and the European Regional Development Fund project TK134 for financial support. Dr. Peter King is appreciated for revising the English of this article.

Received: ((will be filled in by the editorial staff))
Revised: ((will be filled in by the editorial staff))
Published online: ((will be filled in by the editorial staff))

References

[1] G. Sauthoff, in *Intermetallics*, (Eds: P. Gregory, D. Hollis, U. Anton), VCH Verlagsgesellschaft mbH, Weinheim, Federal Republic of Germany, **1995**.

[2] K. A. Benavides, I. W. H. Oswald, J. Y. Chan, *Acc. Chem. Res.* **2018**, *51*, 12.

[3] R. B. van Dover, E. M. Gyorgy, R. J. Cava, J. J. Krajewski, R. J. Felder, W. F. Peck, *Phys. Rev. B* **1993**, *47*, 6134.

[4] B. L. Drake, F. Grandjean, M. J. Kangas, E. K. Okudzeto, A. B. Karki, M. T. Sougrati, D. P. Young, G. J. Long, J. Y. Chan, *Inorg. Chem.* **2010**, *49*, 445.

[5] R. J. Cava, H. W. Zandbergen, B. Batlogg, H. Eisaki, H. Takagi, J. J. Krajewski, W. F. Peck Jr, E. M. Gyorgy, S. Uchida, *Nature* **1994**, *372*, 245.

[6] T. He, Q. Huang, A. P. Ramirez, Y. Wang, K. A. Regan, N. Rogado, M. A. Hayward, M. K. Haas, J. S. Slusky, K. Inumara, H. W. Zandbergen, N. P. Ong, R. J. Cava, *Nature* **2001**, *411*, 54.

[7] H. Hegger, C. Petrovic, E. G. Moshopoulou, M. F. Hundley, J. L. Sarrao, Z. Fisk, J. D. Thompson, *Phys. Rev. Lett.* **2000**, *84*, 4986.

[8] T. Takeshita, W. E. Wallace, R. S. Craig, *J. Catal.* **1976**, *44*, 236.

[9] E. Casado-Rivera, Z. Gál, A. C. D. Angelo, C. Lind, F. J. DiSalvo, H. D. Abruña, *ChemPhysChem* **2003**, *4*, 193.

[10] P. Kamakoti, D. S. Sholl, *J. Memb. Sci.* **2003**, *225*, 145.

[11] Y.-L. Kim, H.-Y. Lee, S.-W. Jang, S.-J. Lee, H.-K. Baik, Y.-S. Yoon, Y.-S. Park, S.-M. Lee, *Solid State Ionics* **2003**, *160*, 235.

[12] N. Mahmood, C. Zhang, F. Liu, J. Zhu, Y. Hou, *ACS Nano* **2013**, *7*, 10307.

[13] J. Shin, W.-H. Ryu, K.-S. Park, I.-D. Kim, *ACS Nano* **2013**, *7*, 7330.

[14] J. Liu, Y. Wen, P. A. van Aken, J. Maier, Y. Yu, *Nano Lett.* **2014**, *14*, 6387.

[15] J. Zhu, D. Deng, *J. Phys. Chem. C* **2015**, *119*, 21323.

[16] B. Huang, J. Yang, Y. Li, S. Xiao, Q. Chen, *Mater. Lett.* **2018**, *210*, 321.

[17] J. Hassoun, S. Panero, B. Scrosati, *J. Power Sources* **2006**, *160*, 1336.

[18] J. Xie, X. B. Zhao, G. S. Cao, J. P. Tu, *J. Power Sources* **2007**, *164*, 386.

[19] J. Hassoun, S. Panero, P. Simon, P. L. Taberna, B. Scrosati, *Adv. Mater.* **2007**, *19*, 1632.

[20] Z. Yi, X. Tian, Q. Han, J. Lian, Y. Wu, L. Wang, *RSC Adv.* **2016**, *6*, 39818.

[21] N. M. Pereira, C. T. Sousa, C. M. Pereira, J. P. Araújo, A. F. Silva, *Cryst. Growth Des.* **2017**, *17*, 5208.

[22] C. Xian, J. Wang, *RSC Adv.* **2018**, *8*, 213.

[23] A. Onda, T. Komatsu, T. Yashima, *Chem. Commun.* **1998**, *2*, 1507.

[24] A. Onda, T. Komatsu, T. Yashima, *Phys. Chem. Chem. Phys.* **2000**, *2*, 2999.

[25] A. Onda, T. Komatsu, T. Yashima, *J. Catal.* **2001**, *201*, 13.

[26] S. Furukawa, K. Ozawa, T. Komatsu, *RSC Adv.* **2013**, *3*, 23269.

[27] M. Ritala, J. Niinistö, in *Chemical Vapour Deposition: Precursors, Processes and Applications*; (Eds: A. C. Jones, M. L. Hitchman), Royal Society of Chemistry, Cambridge, U.K. **2009**, Ch. 4.

[28] S. M. George, *Chem. Rev.* **2010**, *110*, 111.

[29] R. K. Ramachandran, J. Dendooven, M. Filez, V. V. Galvita, H. Poelman, E. Solano, M. M. Minjauw, K. Devloo-Casier, E. Fonda, D. Hermida-Merino, W. Bras, G. B. Marin, C. Detavernier, *ACS Nano* **2016**, *10*, 8770.

[30] R. K. Ramachandran, M. Filez, J. Dendooven, V. V. Galvita, H. Poelman, E. Solano, E. Fonda, G. B. Marin, C. Detavernier, *RSC Adv.* **2017**, *7*, 20201.

[31] A. P. Espejo, R. Zierold, J. Gooth, J. Dendooven, C. Detavernier, J. Escrig, K. Nielsch, *Nanotechnology* **2016**, *27*, 345707.

[32] S. T. Christensen, J. W. Elam, *Chem. Mater.* **2010**, *22*, 2517.

[33] M. J. Weber, A. J. M. Mackus, M. A. Verheijen, C. van der Marel, W. M. M. Kessels, *Chem. Mater.* **2012**, *24*, 2973.

[34] Y. Lei, B. Liu, J. Lu, R. J. Lobo-Lapidus, T. Wu, H. Feng, X. Xia, A. U. Mane, J. A. Libera, J. P. Greeley, J. T. Miller, J. W. Elam, *Chem. Mater.* **2012**, *24*, 3525.

[35] J. Lu, K.-B. Low, Y. Lei, J. A. Libera, A. Nicholls, P. C. Stair, J. W. Elam, *Nat. Commun.* **2014**, *5*, 3264.

[36] S. T. Christensen, H. Feng, J. L. Libera, N. Guo, J. T. Miller, P. C. Stair, J. W. Elam, *Nano Lett.* **2010**, *10*, 3047.

[37] D. Greenslit, E. Eisenbraun, *ECS Trans.* **2011**, *35* (20), 17.

[38] H. Shimizu, Y. Suzuki, T. Nogami, N. Tajima, T. Momose, Y. Kobayashi, Y. Shimogaki, *ECS J. Solid State Sci. Technol.* **2013**, *2*, P311.

[39] H. Shimizu, K. Shima, Y. Suzuki, T. Momose, Y. Shimogaki, *J. Mater. Chem. C* **2015**, *3*, 2500.

[40] L.-G. Wang, Z.-Y. Cao, X. Qian, L. Zhu, D.-P. Cui, A.-D. Li, D. Wu, *ACS Appl. Mater. Interfaces* **2017**, *9*, 6634.

[41] H.-J. Lee, T. E. Hong, S.-H. Kim, *J. Alloys Compd.* **2016**, *686*, 1025.

[42] L. C. Kalutarage, S. B. Clendenning, C. H. Winter, *ECS Trans.* **2014**, *64* (9), 147.

[43] J. Zhang, Y. Xia, *J. Electrochem. Soc.* **2006**, *153*, A1466.

[44] R. E. Cable, R. E. Schaak, *Chem. Mater.* **2005**, *17*, 6835.

[45] A. Yakymovych, H. Ipser, *Nanoscale Res. Lett.* **2017**, *12*, 142.

[46] J. L. Zhang, C. D. Gu, S. Fashu, Y. Y. Tong, M. L. Huang, X. L. Wang, J. P. Tu, *J. Electrochem. Soc.* **2015**, *162*, D1.

[47] A. D. W. Todd, R. A. Dunlap, J. R. Dahn, *J. Alloys Compd.* **2007**, *443*, 114.

[48] T. H.-W. Sun, H.-F. Wang, K.-M. Chi, *J. Mater. Chem.* **2000**, *10*, 1231.

[49] K. Väyrynen, T. Hatanpää, M. Mattinen, M. Heikkilä, K. Mizohata, K. Meinander, J. Räisänen, M. Ritala, M. Leskelä, *Chem. Mater.* **2018**, *30*, 3499.

[50] D. A. Handley, P. B. Hitchcock, G. J. Leigh, *Inorg. Chim. Acta* **2001**, *314*, 1.

[51] D. A. Handley, P. B. Hitchcock, T. H. Lee, G. J. Leigh, *Inorg. Chim. Acta* **2001**, *314*, 14.

[52] M. C. Biesinger, B. P. Payne, A. P. Grosvenor, L. W. M. Lau, A. R. Gerson, R. St. C. Smart, *Appl. Surf. Sci.* **2011**, *257*, 2717.

[53] M. Batzill, D. E. Beck, D. Jerdev, B. E. Koel, *J. Vac. Sci. Technol. A* **2001**, *19*, 1953.

[54] H. S. Sudarminto, K. Sakamoto, Y. Tsuchiuchi, M. Sugisaki, *J. Nucl. Sci. Technol.* **2002**, *39*, 150.

[55] B. S. Lim, A. Rahtu, R. G. Gordon, *Nat. Mater.* **2003**, *2*, 749.

[56] K. J. Blakeney, C. H. Winter, *Chem. Mater.* **2018**, *30*, 1844.

[57] M. C. Morris, H. F. McMurdie, E. H. Evans, B. Paretzkin, J. H. de Groot, C. R. Hubbard, S. J. Carmel, *Nat. Bur. Stand. (U.S.) Monogr.* **1976**, *25*, 92.

The table of contents entry should be 50−60 words long, and the first phrase should be bold.

Intermetallic Co_3Sn_2 and Ni_3Sn_2 are promising materials for Li- and Na-ion batteries and magnetic devices. By combining diamine adducts of Co(II) and Ni(II) chlorides with tributyltin hydride, it is possible to prepare Co_3Sn_2 and Ni_3Sn_2 thin films using atomic layer deposition (ALD). As a precise and controllable method, ALD offers a significant improvement to the previous ways of preparing intermetallics.

Intermetallics

K. Väyrynen, T. Hatanpää, M. Mattinen, K. Mizohata, K. Meinander, J. Räisänen, J. Link, R. Stern, M. Ritala* and M. Leskelä

Atomic Layer Deposition of Intermetallic Co_3Sn_2 and Ni_3Sn_2 Thin Films

Supporting Information

Atomic Layer Deposition of Intermetallic Co_3Sn_2 and Ni_3Sn_2 Thin Films

Katja Väyrynen, Timo Hatanpää, Miika Mattinen, Kenichiro Mizohata, Kristoffer Meinander, Jyrki Räisänen, Joosep Link, Raivo Stern, Mikko Ritala and Markku Leskelä*

Table of Contents

Precursor synthesis

All handling and manipulations were done under rigorous exclusion of air and moisture using standard Schlenk techniques and inert gas (N_2 or Ar) glovebox. Anhydrous $NiCl_2$ (98%, anhydrous, Strem), N,N,N',N'-tetramethylethylenediamine (TMEDA; 99%, Aldrich), and N,N,N',N'-tetramethyl-1,3-propanediamine (TMPDA; 99%, Aldrich) were used as received.

THF was freshly distilled from sodium benzophenone ketyl. Hexane was deoxygenized, dried and stored over 4 Å molecular sieves. Thermogravimetric analyses (TGA) for the nickel compounds were carried out on a Netzsch STA 449F3 Jupiter simultaneous thermal analyzer (STA). The measurements were done using a flowing nitrogen (40 mL/min) atmosphere at 1 atm, and under dynamic vacuum (~0.1 mbar). Melting points were taken from the differential scanning calorimetry (DSC) data measured by the STA. TGA for tributyltin hydride (TBTH, Alfa Aesar) was done using a Mettler Toledo TGA 850 equipment. A flowing N_2 (50 mL/min) atmosphere was used. Mass spectrum was recorded with a JEOL JMS-700 operating in an electron impact mode (70 eV) using a direct insertion probe and a sublimation temperature range of 25−300 °C.

Synthesis of $NiCl_2(TMPDA)$: 3.00 g of $NiCl_2$ (23.148 mmol) was weighed into a 300 mL Schlenk bottle. 150 mL of THF was added. A threefold excess of TMPDA (9.05 g, 69.492 mmol) was then added with a syringe to the stirred suspension. The resulting solution was heated to reflux and stirred overnight. When still warm, the solution was filtered using a Schlenk sinter. The sinter was rinsed with a small amount of THF (30 mL), and the THF filtrates were combined. The purple colored filtrate was evaporated to dryness using a water bath (approx. +50 °C) and vacuum. The resulting purple colored solid was washed with a small amount of hexane and, again, the solid was dried using a water bath and vacuum. The yield of the synthesis at this point was 4.80 g (79.8%). The purple colored product was transferred to a sublimator and sublimed at 150–180 °C/0.4 mbar. 4.43 g of the product was recovered, and the sublimation yield was 92.3%. mp 216 °C; *m/z* (EI, 70 eV) 260 $[M]^+$, 222 $[M\text{-}Cl\text{-}H]^+$, 185 $[M\text{-}2Cl\text{-}3H]^+$, 130 $[L]^+$.

Synthesis of $NiCl_2(TMEDA)_2$: 1.00 g of $NiCl_2$ (7.716 mmol) was weighed into a 300 mL Schlenk bottle. 40 mL of THF was added. An excess of TMEDA (5.0 mL, 33.346 mmol) was then added to the stirred suspension. The resulting solution was heated to reflux for 2 hours. When still warm, the solution was filtered using a Schlenk sinter. The green precipitate left in

the sinter was rinsed with a small amount of THF (30 mL), and the THF filtrates were combined. The orange colored filtrate was concentrated to 10 mL using a water bath (approx. +50 °C) and vacuum. The color of the solution turned yellow. 25 mL of hexane was layered on top of the THF solution. After 16 hours, some yellow crystalline solid had formed at the bottom. The solvents were removed, and the solid was washed twice with 20 mL of hexane. During the second washing, the color of the crystals turned orange. The crystals were dried in vacuum, and the color turned back to yellow. The yield was 0.46 g (24.3%). During the course of attempted sublimation, when heated to 120 °C, the color of the substance at the bottom of the sublimator turned to light green, indicating formation of $[Ni_3Cl_5(TMEDA)_3]Cl$. Then at 150–180 °C, $[Ni_3Cl_5(TMEDA)_3]Cl$ mostly decomposed, and only a very small amount of the sublimate with properties similar with $[Ni_3Cl_5(TMEDA)_3]Cl$ was seen. *m/z* (EI, 70 eV) 246 $[M\text{-}L]^+$, 209 $[M\text{-}L\text{-}Cl]^+$, 171 $[M\text{-}L\text{-}2Cl\text{-}3H]^+$, 116 $[L]^+$.

Figure S1 shows the TGA and DSC curves measured for $NiCl_2(TMPDA)$ under atmospheric pressure of N_2 with a heating rate of 10 °C/min. The residues at 600 °C and at 400 °C are smaller than the theoretical $NiCl_2$ content (49.9 %) of the compound. This indicates partial evaporation of metal containing species.

Figure S2 shows the TG curve for $NiCl_2(TMPDA)$ measured under vacuum with a heating rate of 10 °C/min. The compound mostly evaporates. The residue at 250 °C is 2.4%.

Figure S3 shows the TGA and DSC curves measured for $NiCl_2(TMEDA)_2$ under 1 atm flowing N_2 atmosphere. First, one TMEDA is lost (two first steps, obs. 32.3%, calc. 32.1%), and then the second TMEDA is lost in several phases. The residue at 400 °C is 34.9%, while the theoretical $NiCl_2$ content of the compound is 35.8%.

Figure S4 shows the TG curves measured for tributyl tin hydride (TBTH, Alfa Aesar). The curves were measured under 1 atm flowing N_2 atmosphere using either an open crucible (heating rate of 10 °C/min) or using a crucible with a lid that has a small orifice (heating rate 5 °C/min and 25 °C/min). The samples were loaded into the crucibles in a nitrogen filled

glovebox, but the loading of the crucibles into the TG equipment was done in air. Here, the idea of using crucibles with a lid was to protect the sensitive sample from damage caused by air and moisture while loading the sample into the TGA equipment. The idea of using the crucible with a lid and the high heating rate was to restrict the evaporation of the compound and cause the sample to experience a higher temperature before evaporation; if the use of the higher heating rate resulted in a higher residue than with the lower heating rate, thermal decomposition could be concluded. TBTH is highly sensitive to air and moisture; thus, loading the samples inevitably resulted in sample damage, more so in the case of open crucibles. The larger residue and larger second step seen in the TGA curve measured using the open crucible are explained by the air and moisture sensitivity of TBTH. The size of the second step seen in all the curves seems to depend on the exposure to air and moisture. As expected, the TG curve measured with the fast heating rate (25 °C/min) shows two steps at higher temperatures as compared with the curves measured with 5 °C/ min (crucible with lid) and 10 °C/min (open cup) heating rates. The smaller second step indicates smaller damage to the sample due to air and moisture predisposure. The larger residue indicates thermal decomposition. With the 5 °C/min heating rate and the crucible with a lid there is zero residue, again indicating the absence of thermal decomposition. Considering the data from different TG measurements done for TBTH, it seems that the thermal decomposition of bulk material is insignificant or absent at least at temperatures below 200 °C.

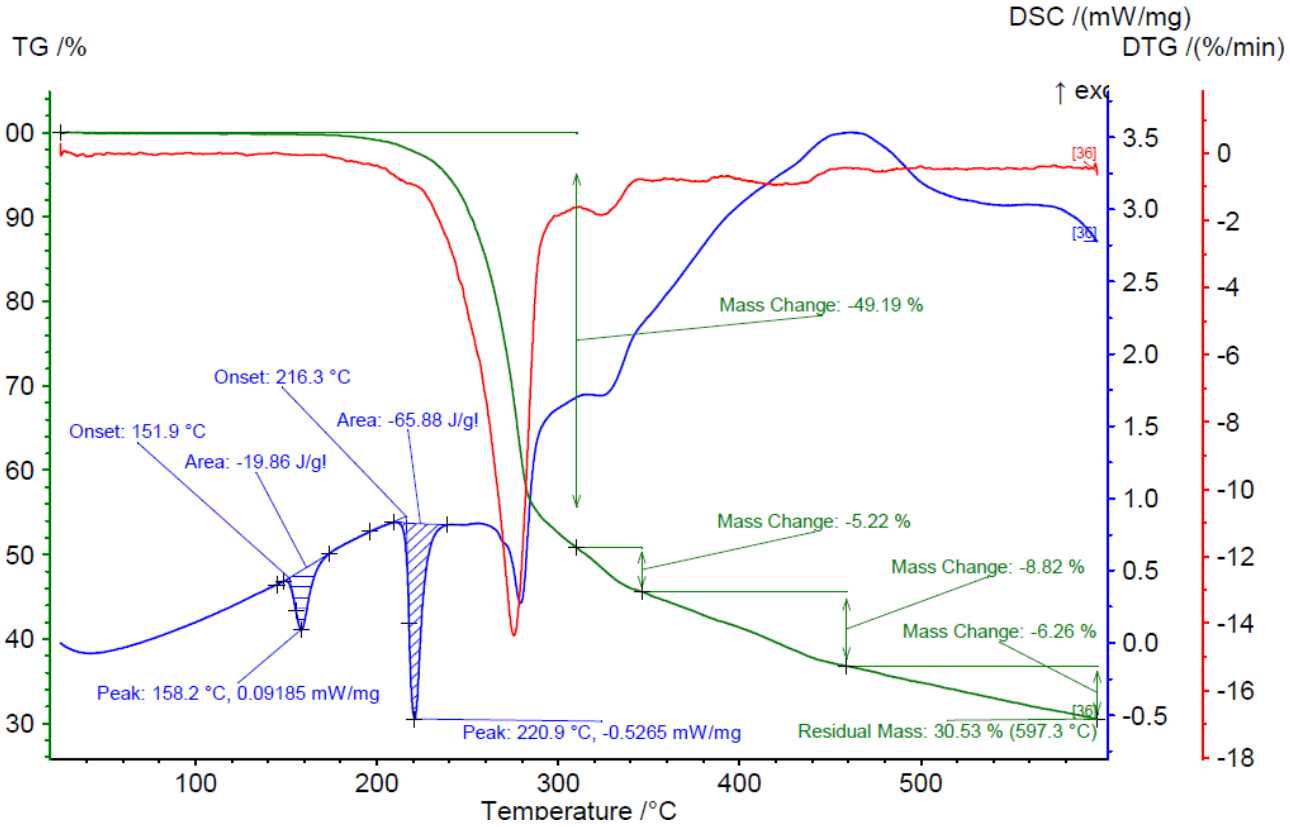

Figure S1. TGA and DSC curves measured for $NiCl_2$(TMPDA) under 1 atm flowing N_2 atmosphere with a heating rate of 10 °C/min.

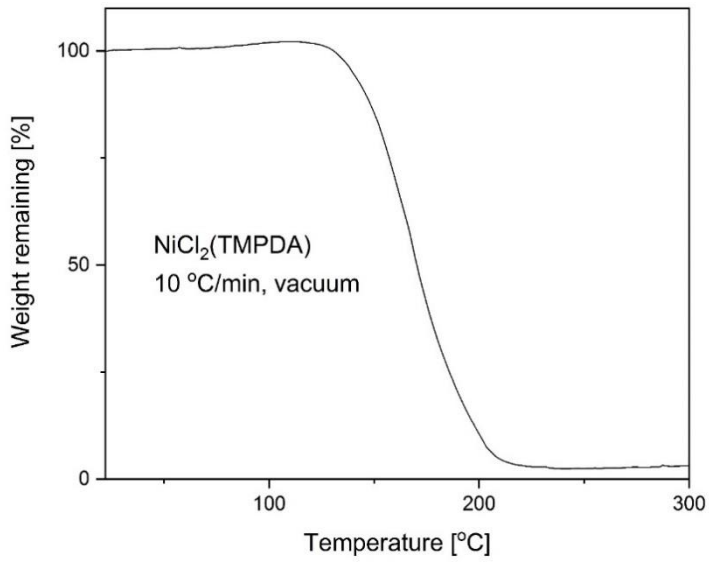

Figure S2. TG curve for $NiCl_2$(TMPDA) measured under vacuum with a heating rate of 10 °C/min.

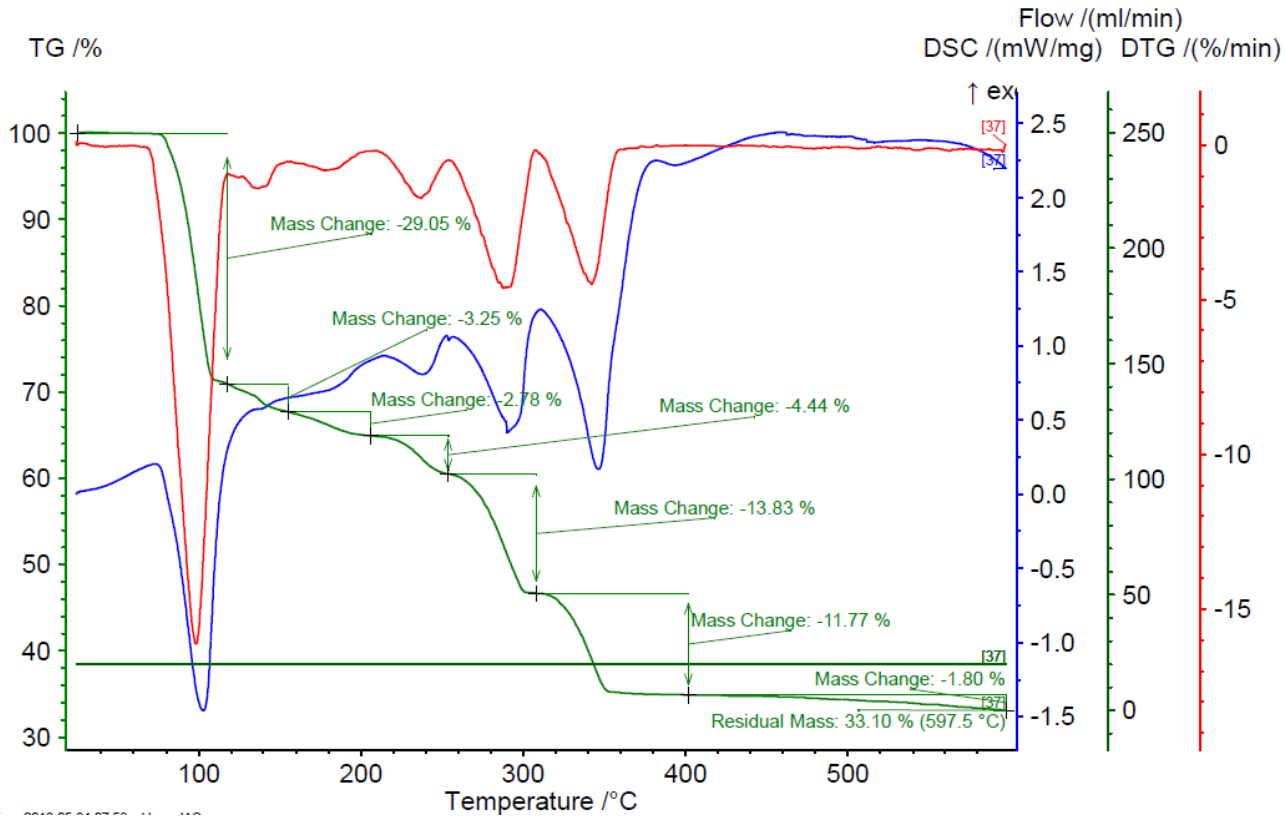

Figure S3. TGA and DSC curves measured for $NiCl_2(TMEDA)_2$ under 1 atm flowing N_2 atmosphere with a heating rate of 10 °C/min.

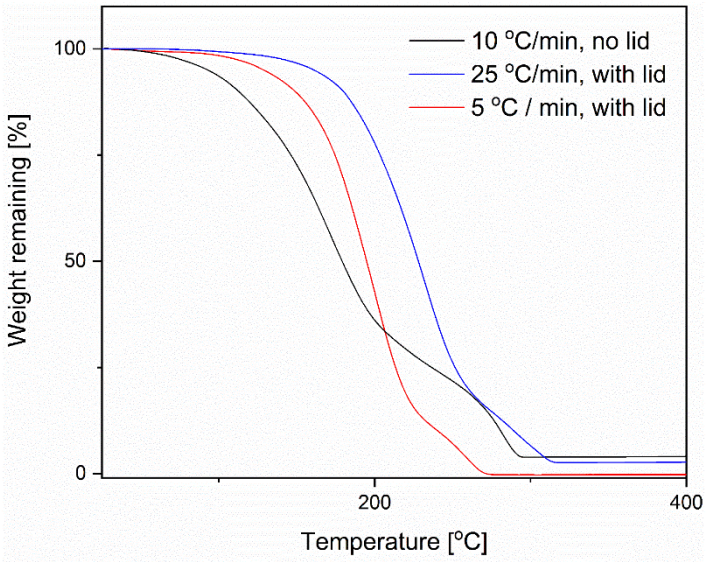

Figure S4. TG curves measured for TBTH (Alfa Aesar). The curves were measured under 1 atm flowing N_2 atmosphere using a heating rate of 10 °C/min and an open crucible (black), using a heating rate of 5 °C/min and a crucible with a lid that has a small orifice (red), and using a heating rate of 25 °C/min and a crucible with a lid that has a small orifice (blue).

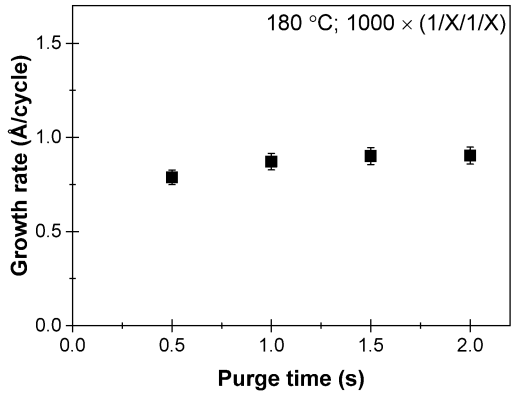

Figure S5. Growth rate of Co_3Sn_2 with respect to purge times at 180 °C. The deposition comprised 1000 cycles and 1.0 s precursor pulse lengths.

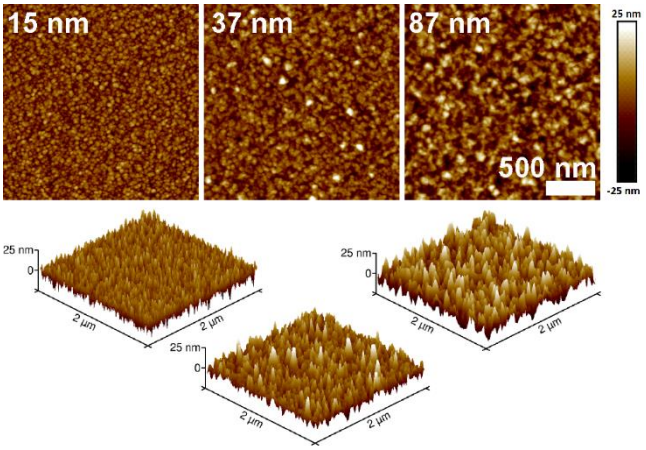

Figure S6. AFM images of Co_3Sn_2 films (15, 37, and 87 nm) deposited at 180 °C.

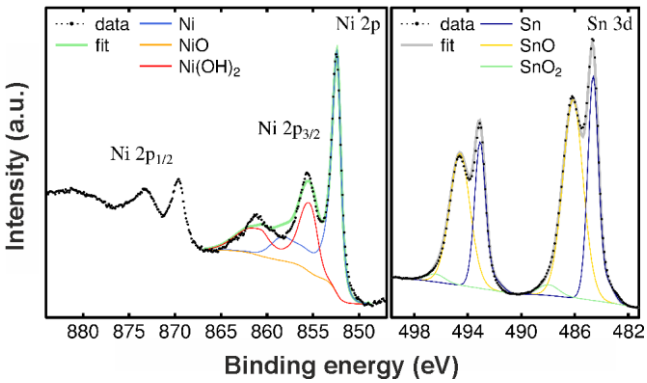

Figure S7. Ni 2p and Sn 3d X-ray photoelectron spectra of a 127 nm Ni_3Sn_2 film deposited at 160 °C.

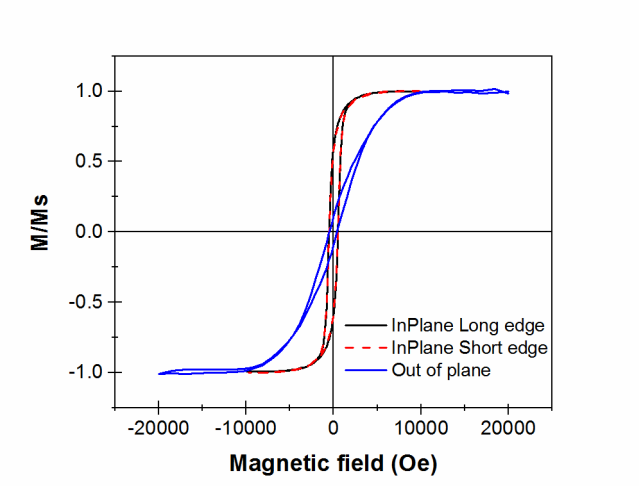

Figure S8. Co_3Sn_2 magnetic measurements in different orientations (two in-plane and one out-of-plane measurement).

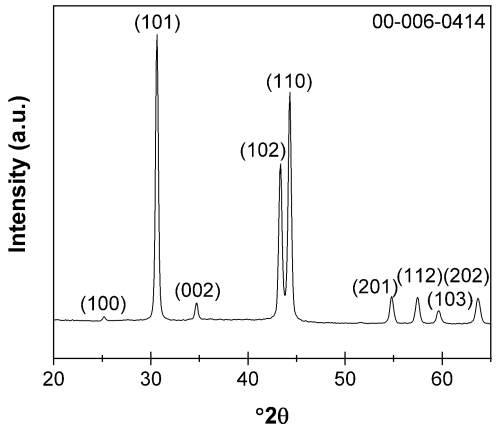

Figure S9. Grazing incidence X-ray diffractogram of a 127 nm Ni_3Sn_2 thin film deposited at 160 °C.

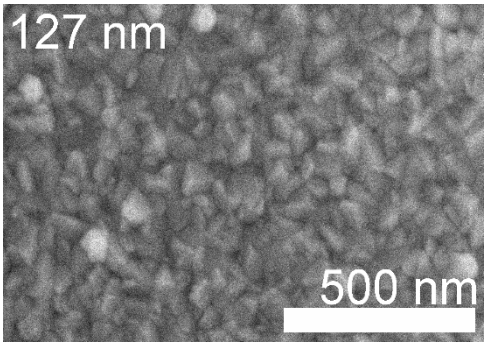

Figure S10. SEM image of a 127 nm Ni_3Sn_2 thin film deposited at 160 °C.

Table S1. ToF-ERDA results (at.%) from a 127 nm Ni_3Sn_2 film deposited at 160 °C.

Element	160 °C
Ni	59.4 ± 0.4
Sn	38.9 ± 0.3
H	0.6 ± 0.2
C	0.15 ± 0.03
N	0.07 ± 0.02
O	0.95 ± 0.07